METHODS

CMEIAS Color Segmentation: An Improved Computing Technology to Process Color Images for Quantitative Microbial Ecology Studies at Single-Cell Resolution

Colin A. Gross · Chandan K. Reddy · Frank B. Dazzo

Abstract Quantitative microscopy and digital image analysis are underutilized in microbial ecology largely because of the laborious task to segment foreground object pixels from background, especially in complex color micrographs of environmental samples. In this paper, we describe an improved computing technology developed to alleviate this limitation. The system's uniqueness is its ability to edit digital images accurately when presented with the difficult yet commonplace challenge of removing background pixels whose three-dimensional color space overlaps the range that defines foreground objects. Image segmentation is accomplished by utilizing algorithms that address color and spatial relationships of user-selected foreground object pixels. Performance of the color segmentation algorithm evaluated on 26 complex micrographs at single pixel resolution had an overall pixel classification accuracy of 99+%. Several applications illustrate how this improved computing technology can successfully resolve numerous challenges of complex color segmentation in order to produce images from which quantitative information can be accurately extracted, thereby gain new perspectives on the in situ ecology of microorganisms. Examples include improvements in the quantitative analysis of (1) microbial abundance and phylotype diversity of single cells classified by their discriminating color within heterogeneous communities, (2) cell viability, (3) spatial relationships and intensity of bacterial gene expression involved in cellular communication between individual cells within rhizoplane biofilms, and (4) biofilm ecophysiology based on ribotype-differentiated radioactive substrate utilization. The stand-alone executable file plus user manual and tutorial images for this color segmentation computing application are freely available at http://cme.msu.edu/cmeias/. This improved computing technology opens new opportunities of imaging applications where discriminating colors really matter most, thereby strengthening quantitative microscopy-based approaches to advance microbial ecology in situ at individual single-cell resolution.

C. A. Gross · F. B. Dazzo (✉)
Department of Microbiology & Molecular Genetics,
Michigan State University,
East Lansing, MI 48824, USA
e-mail: dazzo@msu.edu

C. K. Reddy · F. B. Dazzo
Center for Microbial Ecology,
Michigan State University,
East Lansing, MI 48824, USA

Present Address:
C. A. Gross
Surgery Branch, National Cancer Institute,
National Institutes of Health,
Bethesda, MD 20814, USA

Present Address:
C. K. Reddy
Department of Computer Science,
Wayne State University,
Detroit, MI 48202, USA

Introduction

Microscopy and digital image analysis are important investigative tools in microbial ecology that provide direct quantitative information on the microbes' world from their own perspective and spatial scale without the need for their laboratory cultivation [4, 6, 7]. Unfortunately, much less information than actually available in images of microbes has been obtained using computer-assisted microscopy, primarily because digital images of microorganisms in their natural habitats are highly complex, posing major challenges of image processing required for quantitative image

Ⓐ Springer

analysis [26]. An essential and most difficult task is object segmentation, which represents all editing steps required to reduce the image to the foreground objects (microbes) of interest before analysis. Complexity of image segmentation is increased even further when the organisms are colored to reveal important information on their ecological, biochemical, physiological, cytological, and/or phylogenetic characterics in situ (Fig. 1). As a consequence, information on the richness, abundance, metabolic activity, and spatial heterogeneity of microbial populations and communities in complex environments is often visually described but rarely quantitated from true bitmap color images, compromising the potential impact of the study itself.

The challenge of color segmentation is how to separate foreground pixels from background along fine delineations of color and location within the complex image. The underlying problem is that microbial objects of interest in high definition, digital color images are commonly represented by pixels with *heterogeneous* brightness ranges of red, green, and blue (RGB) that most often also include colored pixels of background at similar locations, and the pixels often have shallow gradients of brightness transition at cell borders resulting in indistinctive boundaries that contrast gradually with the background. This digital heterogeneity may not be noticeable when the image is viewed at 1:1 (100% zoom), but is obvious when magnified to view the color of individual pixels comprising the microbial objects (Fig. 2). Solving this challenging segmentation problem is crucial when any computer-assisted microscopy application uses color information (Fig. 1) to extract ecologically relevant quantitative data, especially at the resolution of individual microbial cells within environmental samples.

Most often, color segmentation of microbial images is addressed by isolating the foreground object pixels with a single or narrow RGB color range and/or splitting the color image into its individual RGB chromatic channels followed by thresholding the channel that contains the most intense signals for the targets of interest while suppressing the intensity of the other channels [28]. This approach has variable degrees of success when applied to digitally pseudocolored monochrome images, such as those acquired as a primary grayscale image using confocal laser scanning microscopy and then pseudocolor processed for specific fluorochromes. Implementing other image processing routines such as dilation/erosion, Gaussian blur, contrast manipulation, spatial convolution masks, c-means clustering, classification of pixels into predefined pseudochannel classes, mean–median filtering, and measurement feature descriptors for object size and/or shape filtration can sometimes help to minimize blurred object edges and complement color channel-based image segmentation of microbes [1, 2, 9, 11, 13, 24, 25, 29, 30]. However, combinations of these image processing routines rarely succeed in segmenting the three-dimensional color space that accurately defines all foreground pixels of microbial targets of interest at all locations within complex, true bitmap color images to analyze their size, shape, abundance, and spatial location in situ. In addition, underlying assumptions (e.g., RGB intensities of foreground object pixels are approximately equal to each other and greater than intensities of background objects) are not always valid, and the original true color intensities of the foreground objects are inevitably lost using these routines since they are typically applied to the whole image even when only selected areas require them.
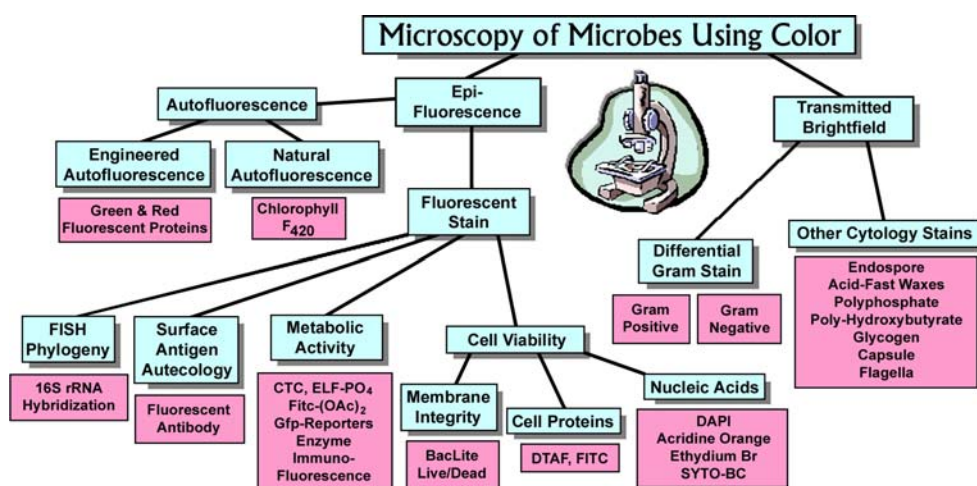

Figure 1 Hierarchical organization of various types of epifluorescence and transmitted light microscopy that utilize the discriminating power of color information to reveal significant characteristics of microorganisms. *FISH*, fluorescent in situ hybridization, *CTC* (5-cyano-2,3-ditolyl-tetrazolium chloride), *FITC* fluorescein isothiocyanate, *Gfp* green fluorescent protein, *DTAF* 5-(4,6)-dichlorotriazinyl-aminofluorescein, *DAPI* 4′,6-diamidino-2-phenylindole dihydrochloride. ELF™-PO₄ and SYTO™ BC are commercial trademarks
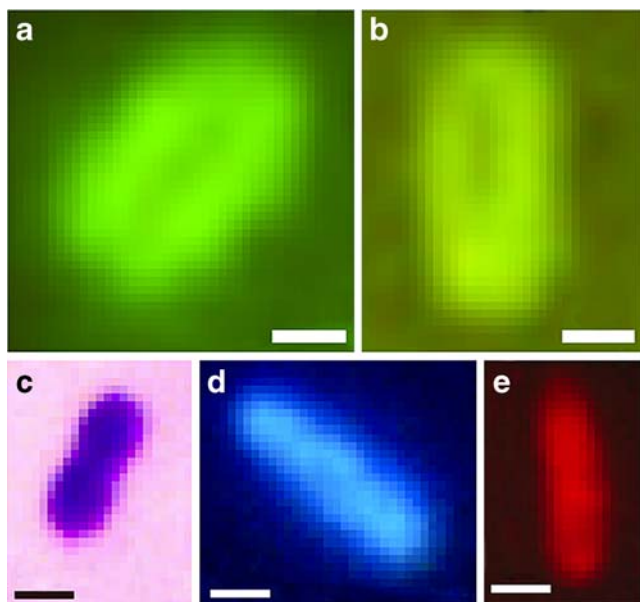
Figure 2 Zoomed-in detail of digital images showing variation in pixels comprising individual bacterial cells and the indistinct fluorescent halo surrounding their boundaries (due to the bending of light as it passes through the cell). The color stains and their corresponding RGB ranges are: **a** FITC r92-r118, g198-g255, b0; **b** DTAF r116-r179, g166-g246, b167-b227; **c** crystal violet r62-r157, g0, b167-b227; **d** DAPI r1-r74, g49-g191, b157-b255; **e** rhodamine r124-r217, g0, b1-b8. *Bar scales*, 0.5 μm

Previously, we described a color segmentation algorithm to process and mine data from color images of microbes [22, 23]. However, its further testing revealed two significant limitations. The first was its inability to successfully classify foreground pixels when pixels of background differed only in spatial density, e.g., populations stained with 4′-6-diamidino-2-phenylindole (DAPI), fluorescence in situ hybridization (FISH), immunofluorescence, or contained reporter strains expressing genes encoding fluorescent protein(s) while colonized on plant roots that exhibited autofluorescence of the same color but at lower pixel density. The second was that it could not adequately distinguish different microbial populations with similar color contents (e.g., red vs. orange fluorescent bacteria stained with acridine orange).

The objective of this study was to minimize these limitations by developing a more accurate, efficient, robust, and versatile algorithm to semi-automate the segmentation of multicolored microbes in digitized color images that also contain complex and usually noisy backgrounds and to implement this improved technology into a well-documented and user-friendly PC software application. Here, we describe the computer vision logic of our new system, the accuracy of its significantly improved color segmentation algorithm, and examples of its application to solve various complex image processing challenges commonly encountered in color images acquired for quantitative microbial ecology studies. This free computing toolkit will facilitate the integration of microbial ecology with cutting edge "individual single-cell microbiology" at spatial scales directly relevant to the microorganisms themselves. Portions of this work were described at the 11th International Society for Microbial Ecology symposium (2006, Vienna, Austria).

Materials and Methods

Test Images

Brightfield transmitted and epifluorescence microscopies were used to acquire color images from various complex microbial communities, including methanogenic anaerobic bioreactors, activated sludge, rhizoplane, mycorrhizosphere, canine feces, human nasopharynx, and estuary. When very high resolution of pixel sampling density was needed, images were acquired on Kodak Elite Chrome 100- or 400-ASA photographic slide films using a Zeiss Photomicroscope I equipped with 100× Neofluor and Planapochromat oil immersion objective lenses and converted to 24-bit RGB, uncompressed 1,200 dpi digital Tiff images using an Epson Perfection 4180 photoscanner. Other color micrographs were acquired directly using a Cannon 10D digital SLR camera. Table 1 lists the image name, stain/method and type of light microscopy used, the cell component or activity that is differentiated by color, and the source.

Ground truth images were prepared by manually editing the color images using Adobe Photoshop™ or GNU Image Manipulation Program (GIMP) so that all foreground pixels of microbial cells were separated from noise-free background. Examples of ground truth images are shown in Fig. 3.

Figures 1, 2, 3, 4, 5, 6, 7, 8, 9, 10, 11, and 12 are presented in color at the Online First webpage of this Microbial Ecology article.

Software Development and Image Analysis

The software toolkit to implement the color segmentation algorithm plus accessory image processing routines was written in Visual C++ using Microsoft™ Visual Studio ver. 6.0. A separate segmentation accuracy analysis tool was developed in C++ to automate the full pixel-by-pixel color comparison of test result images and the corresponding ground truth images, followed by computation of the accuracy values for each image. For quantitative image analysis, color-segmented images were converted to 8-bit grayscale Tif images and analyzed with Center for Microbial Ecology Image Analysis Software (CMEIAS, 6, 19) operating within UTHSCSA ImageTool (Univ. Texas Health Science Center, San Antonio, TX. http://ddsdx.uthscsa.edu/dig/itdesc.html).

Table 1 24-bit RGB color images used in this study

Image	Stain/Microscopy method	Sample/Differentiated target	Source
AcriOrig-1	Acridine Orange/Epifluorescence	*Pseudomonas* sp./Nucleic acid	E. Polone
BacLight-1	LiveDead BacLight/Epifluorescence	*Micrococcus luteus, B. cereus*/Via.	Molec. Probes
BacLight-2	LiveDead BacLight/Epifluorescence	*Yersinia pestis*/Via.	T. Marsh
BcFitcTritc-1	FITC + TRITC/Epifluorescence	*Bacillus cereus*/spore proteins	G. McFeters
DAPI-1	DAPI/Epifluorescence	*Pseudomonas* sp./Nucleoid	This study
DAPI-2	DAPI/Epifluorescence	*Pseudomonas* sp./Nucleoid	This study
DAPI-3	DAPI/Epifluorescence	*Pseudomonas* sp./Nucleoid	This study
DAPI-4	DAPI/Epifluorescence	*Pseudomonas* sp./Nucleoid	This study
DAPI-5	DAPI/Epifluorescence	*Pseudomonas* sp./Nucleoid	This study
DAPI-6	DAPI/Epifluorescence	Anaerobic bioreactor/Nucleoid	S. Dolhopf
DAPI-7	DAPI/Epifluorescence	*Pseudomonas* sp./Nucleoid	R. Schumann
DAPI-Fish-1	DAPI + FISH epifluorescence	*Pseudomonas* sp./Nucleoid + 16S rRNA	This study
Fish-2	FISH epifluorescence	Spirochete + *Clostridium*/16S rRNA	S. Dolhopf
Fish-3	FISH epifluorescence	Spirochete + *Clostridium*/16S rRNA	S. Dolhopf
Fish-4	FISH epifluorescence	Spirochete + *Clostridium*/16S rRNA	S. Dolhopf
Fish-5	FISH epifluorescence	Spirochete + *Clostridium*/16S rRNA	S. Dolhopf
Fish-6	FISH epifluorescence	Spirochete + *Clostridium*/16S rRNA	S. Dolhopf
GeneExp-1	Gfp + Rfp expression/Epifluorescence	*P. putida*—roots/Reporter gene	S. Gantner
GeneExp-2	Gfp + Rfp expression/Epifluorescence	*P. putida*—roots/Reporter gene	S. Gantner
GeneExp-3	Gfp + Rfp expression/Epifluorescence	*P. putida*—roots/Reporter gene	S. Gantner
GS-1	Gram stain/Brightfield	Bacteremia/Cell wall	ASM
GS-3	Gram stain/Brightfield	Canine diarrhea/Cell wall	This study
GS-5	Gram stain/Brightfield	Nasopharynx/Cell wall	This study
IFM-1	FITC-antibody/Epifluorescence	*Rhizobium leguminosarum* Surface antigen	This study
NatAuto-1	Autofluorescence/Epifluorescence	Algae + Cyanobacteria Chorophyll A	This study
NatAuto-2	Autofluorescence/Epifluorescence	Algae + Cyanobacteria Chorophyll A	This study
MRZ-Com	Fish Multiprobe/Epifluorescence	Mycorrhizal fungus + Multiprobe 16S rRNA + autofluorescence	M. Schmid
Fish-Mar Fish Epifluor.	Microautoradiography	*Nitrospira* sp./16S rRNA	H. Daims

Gfp green fluorescent protein, *Rfp* red fluorescent protein, *Via.* viability–membrane integrity, *ASM* American Society for Microbiology Image Archive
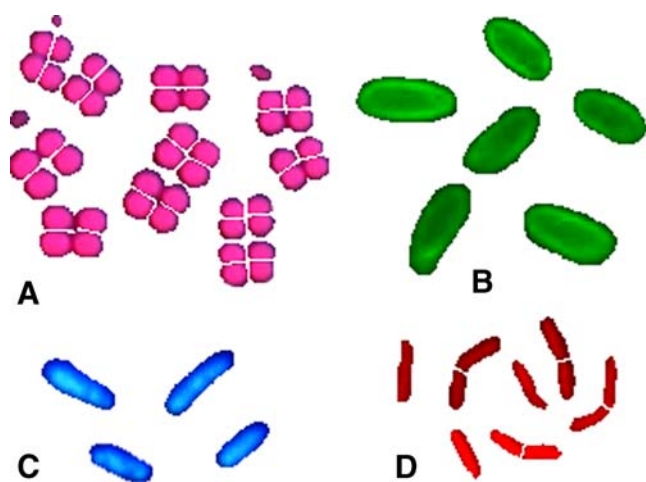

Figure 3 Examples of bacterial cells in ground truth images used to evaluate the performance and accuracy of the color segmentation algorithm. Fluorescence due to **a** autofluorescent pigments, **b** FITC, **c** DAPI, and **d** TRITC

General Color Segmentation Protocol

Figure 4 presents the general sequence of steps to segment color images using our new system. First, images are opened and examined to assess the color heterogeneity of foreground object pixels and their contrast to background. Six different cursor designs were provided to optimize the precision of that evaluation. The RGB values of the pixel under the cursor automatically display in the status bar, providing the information used to set the color tolerance on a scale that defines the range of colors to be included in foreground pixels near each sampled pixel's location. Next, "training" pixels are interactively and carefully sampled from the objects of interest in each region of similar color within the active image. The required number of training pixels depends on their color heterogeneity within the foreground objects and how isolated are those regions within the image. Doing this pixel sampling task while viewing the cells in a
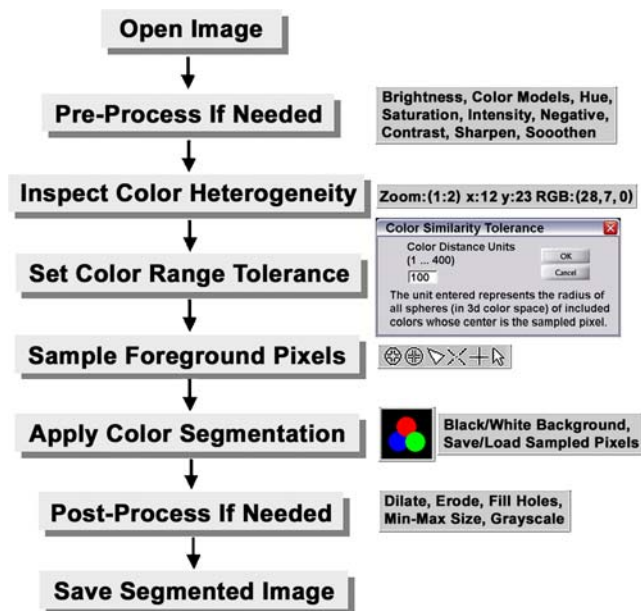
Open Image

Pre-Process If Needed

Brightness, Color Models, Hue, Saturation, Intensity, Negative, Contrast, Sharpen, Sooothen

Inspect Color Heterogeneity

Zoom: (1:2) x:12 y:23 RGB:(28, 7, 0)

Set Color Range Tolerance

Color Similarity Tolerance

Color Distance Units
(1 ... 400)
100

OK
Cancel

The unit entered represents the radius of all spheres (in 3d color space) of included colors whose center is the sampled pixel.

Sample Foreground Pixels

Apply Color Segmentation

Black/White Background, Save/Load Sampled Pixels

Post-Process If Needed

Dilate, Erode, Fill Holes, Min-Max Size, Grayscale

Save Segmented Image

Figure 4 General sequence of steps to segment the foreground objects in images using the CMEIAS color segmentation application

zoom mode can be helpful. The time required to complete this step will depend on the size and complexity of the image, number of foreground sample points needed to represent the target group, and whether the foreground signal and background noise of the currently active image are sufficiently similar to previously segmented images whose array of sampled training pixels had been saved.

Once these interactively trained inputs are registered, the color segmentation algorithm is activated to analyze the image, pixel-by-pixel, using the color and spatial ranges specified by the user-selected training pixels and the input of the threshold value that defines their three-dimensional color space to determine which pixels are to be included as foreground objects. The computing time to run the segmentation algorithm is reported in milliseconds in the status bar and was typically less than 2 s for each test image included in this study (computer specs: Pentium 4, 3.00 GHz CPU, 2 GB RAM). After the pixel classification is completed, the system automatically creates and displays a new color segmentation output image with the pixels of foreground objects retained in their original color and position and the non-foreground pixels painted either black or white (user-specified) to create the optimally contrasted, noise-free background. Subsequent iterations of this sequence plus combinations of other image post-processing features in the system (Fig. 4) can be applied as necessary to refine the results of the output image and produce the final image segmentation desired. When displayed, the segmented 24-bit RGB output image or its 8-bit grayscale image derivative can be saved directly as is or copied to the Window's clipboard.

Testing the Color Segmentation Algorithm

Measurement of the accuracy of the color segmentation algorithm was based on the degree to which its automatic classification output of colored pixels made solely using user-selected training pixels matched their accepted assignments for the corresponding target objects in a pixel-by-pixel comparison to the ground truth images. Color segmentation errors were of two types (Fig. 5). In our computer vision-based approach, we assigned a false dismissal (i.e., false negative) error to any pixel that was classified as background in the output image but treated as foreground at the corresponding location in the ground truth image [27]. In this case, the foreground object pixel is missing in the output image. Conversely, we assigned a false alarm (i.e., false positive) error to any pixel that was included as foreground in the segmented output result image but was classified as background at the same location in the ground truth image [27]. The error rate of the color segmentation functionality was calculated as the sum of all incorrectly classified pixels divided by the total number of pixels in the same image, reported as the total percent of error.

Results and Discussion

The System Logic of CMEIAS Color Segmentation

At the core of this improved computing technology is the color segmentation algorithm implemented to use "instance-based learning" logic to decide whether each image pixel was foreground or background. It does this by evaluating and classifying the local neighborhoods of
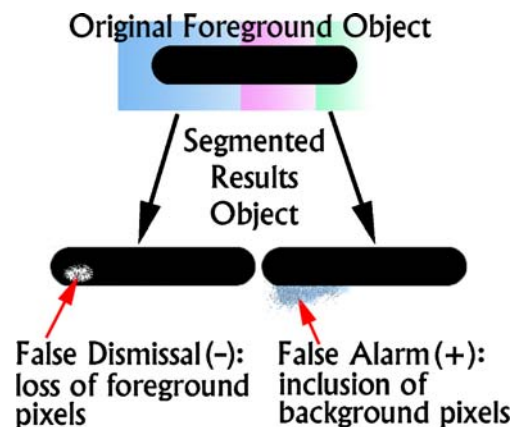
Original Foreground Object

Segmented Results Object

False Dismissal (−): loss of foreground pixels

False Alarm (+): inclusion of background pixels

Figure 5 Schematic diagram illustrating the false dismissal (false negative) and false alarm (false positive) pixel errors that were differentially measured to evaluate the accuracy of the color segmentation algorithm

pixel-forming patches of related color features in the image grid. The knowledge it requires to produce the optimal color segmentation output is provided by carefully sampled training points whose color and spatial position accurately represent the range of features of the desired target group. After sampling, the image is projected into three-dimensional RGB color space, and the distances between the specific three color-coordinate positions of each image pixel and the training sample pixels are measured. Next, the two-dimensional spatial distance between each image pixel and its nearest sampled point is measured, followed by using the distance-weighted similarity function to combine both the color and spatial distances. Then, the segmentation routine is performed within a single pass of operation using these color and spatial comparison analyses to segment the nearest neighbor (physical location) comparison analysis of a user-selected pixel in relation to the location of other pixels within the image. Without these latter components of the color segmentation algorithm, pixels of background with color similar to the foreground objects would misclassify as included and therefore fail to achieve the desired goal. The unique features of these weighted similarity measurements provide a level of functionality and flexibility not available previously or elsewhere, and therefore, this new system represents an improvement in existing technology that is well suited to successfully segment the foreground objects in complex images that contain multiple regions of interest with different color ranges. The latter complex situation is the normal case commonly encountered for in situ microbial community analysis of environmental samples.

The most significant feature added to address the limitations of our earlier CMEIAS prototypes [22, 23] was a method enabling the user to specify the threshold of color inclusion in order to optimize the color segmentation functionality. This user-define threshold setting controlled the radial distance of the three-dimensional quasi-spherical color space that each neighboring pixel in the image could deviate from the color of the user-selected pixel and still be included as a foreground pixel in the output result image. New adjustments in the threshold setting for the color comparison function either narrow or expand the RGB color space relative to the previous threshold setting used in the segmentation algorithm. The "Save/Load Sampled Pixels" and "Edit Undo/Redo" features facilitate the optimization of the color tolerance limit using iterations of trial and error, thereby increasing the accuracy of the final segmented image output. The added utility to vary the color similarity tolerance function before implementing color segmentation is akin to the increased cutting accuracy achieved using a surgeon's thin scalpel blade instead of an axe. Another benefit is its ability to deblur and restore foreground signals to images with spherical aberration errors near the edge of the circular microscope field.

Performance Accuracy of Color Segmentation

Thirty image segmentation tests were evaluated on 26 different images, producing a total test sample size of 9,115,165 pixels that were each analyzed and classified individually. In four cases, two different subpopulations of microbes within the same image were classified by their fluorescent colors, e.g., red vs. orange cells using acridine orange, and combinations of Fitc/Tritc, Gfp/Rfp as reporters of gene expression and DAPI/FISH.

This new algorithm classified the image foreground pixels with an overall average segmentation accuracy of 99.343% (Table 2). The error rate ranged from 0.086% to 2.846% per image, with 80% of the images having error rates of less than 1% and all but one image having error rates of less than 2%. These results provide a strong validation of the semi-automated color segmentation algorithm featured in the system.

Detailed comparisons of the ground truth and result image outputs indicated that the color segmentation function had a very high signal-to-noise ratio from which accurate quantitative analysis of the foreground microbial targets could be extracted. However, occasionally, the system selected boundaries with an indistinct fluorescent halo surrounding cells (Fig. 2) that were slightly different from the boundary defined by human intervention to obtain ground truth data, even though the shape of the segmented foreground object remained very similar in both image outputs. This test result emphasized the importance of accurately sampling a sufficient number of foreground training points for every variable region of color to achieve successful color segmentation of complex images with minimal error.

Post-processing features were included in the system (Fig. 4) to correct the segmentation errors when encountered. For example, color dilation and erosion function-alities corrected most false alarm errors, and the "Fill Small Holes" feature corrected most false dismissal errors. The latter feature automatically converted internal foreground pixels lost during color segmentation into the object's average color, and the upper size limit of the color-processed hole could be user-specified and optimized.

Applications of this Computing Toolkit in Studies of Microbial Ecology

The efficacy of this improved computing technology was examined by evaluating its ability to resolve four major categories of image segmentation challenges encountered when using color images in studies of microbial ecology. In each example, color segmentation could not be adequately resolved for accurate quantitative image analysis by the commonly used routines of isolating the foreground pixels

Table 2 Accuracy testing of the CMEIAS color segmentation algorithm

Image name	False (−) dismissal pixels	False (+) alarm pixels	Total pixels in error	Total image pixels	% Error
AcriOrg-1[a]	103	1,363	1,456	304,570	0.478
AcriOrg-1[a]	677	5,238	5,915	304,570	1.942
BacLite-1	1,824	808	2,632	232,000	1.134
BacLite-2	5,018	3,017	8,036	654,225	1.228
BcFitcTritc-1[a]	150	642	792	186,835	0.424
BcFitcTritc-1[a]	462	84	546	186,835	0.292
Dapi-1	779	727	1,506	137,740	1.093
Dapi-2	0	455	455	15,985	2.846
Dapi-3	2	52	54	11,990	0.450
Dapi-4	47	103	150	48,391	0.301
Dapi-5	262	704	966	297,568	0.325
Dapi-6	1,230	615	1,845	388,644	0.474
Dapi-7	264	1,762	2,026	187,982	1.078
DapiFish-1[a]	141	1	142	128,400	0.111
DapiFish-1[a]	29	82	111	128,400	0.086
Fish-2	0	164	164	34,322	0.478
Fish-3	117	140	257	49,851	0.516
Fish-4	141	1	142	44,880	0.317
Fish-5	133	168	301	124,033	0.242
Fish-6	1,073	1,076	2,149	328,229	0.655
GeneExp-1	374	1,472	1,846	727,716	0.254
GeneExp-2	92	104	196	54,384	0.360
GeneExp-3[a]	58	1,585	1,643	727,902	0.226
GeneExp-3[a]	513	2,887	340	727,902	0.467
Gram-1	253	946	1,199	185,129	0.648
Gram-3	8	259	267	62,444	0.428
Gram-5	54	2,879	3,033	461,660	0.660
IFM-1	188	163	351	57,658	0.609
NatAuto-1	7,465	6,943	14,408	1,610,172	0.895
NatAuto-2	4,243	591	4,834	704,748	0.686

Pertinent information on each image is summarized in Table 1

[a] Images with multiple populations of cells classified by color segmentation

of microbial targets using a single or a small range of RGB value(s) and/or by splitting the color image into its individual RGB chromatic channels followed by thresholding the channel(s) that contain(s) the most intense signals for the targets of interest while suppressing the intensity of the other channel(s).

The most widespread challenge in segmenting color images arose when the pixels of foreground objects and background were similar in color hue but varied in luminosity. This commonly occurred when microbes were stained with DAPI, hybridized with fluorescent 16S rRNA-derived oligonucleotide probes, or expressed autofluorescent components like chlorophyll, F_{420}, or Gfp (Fig. 1). This imaging problem manifested because the target components (e.g., nucleoids and ribosomes) were hetero-geneously distributed within the cell when sampled, photo sensors in the digital camera registered incorrect RGB values of background under low light conditions, the background substratum absorbed some stain, and/or the environmental samples contained similarly autofluorescent detritus.

Various strategies were used to resolve this category of image processing challenges depending upon the specific cause. In the first example, microbial cells stained with DAPI exhibited heterogeneity in their internal luminosity (Fig. 6a). This challenge was solved by selecting several training pixels from neighboring cells, including some that have a color value located midway between the most common values of the foreground objects, thereby produc-ing the color segmented result image that retained the
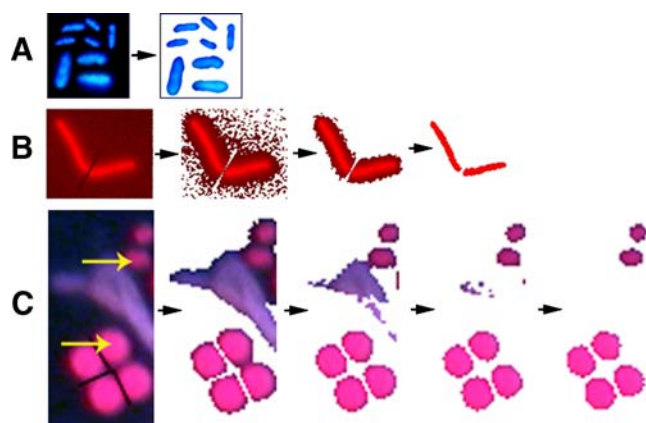
Figure 6 Image processing sequences to isolate the foreground objects of interest by color segmentation when the foreground and background pixels are similar in color hue but vary in luminosity. Examples (*top to bottom*) are: **a** *Pseudomonas* sp. stained with DAPI for cell density counting, **b** FISH of a *Clostridium* sp. in an anaerobic bioreactor community, **c** autofluorescent cyanobacteria in an estuary sample. *Black right arrowheads* show the progression of image processing iterations applied to achieve final segmentation

number, size, shape, and spatial location of the cells in the original image. The overall average accuracy rate for color segmentation of DAPI-stained bacteria using our system was 99.3% ($n=9$, Table 2).

The next two examples in this first category of color segmentation challenge took advantage of the flexible design of the color similarity tolerance tool. In Fig. 6b, the FISH image of *Clostridium* cells in the anaerobic bioreactor was very noisy, containing foreground pixels afloat in a background of similarly colored pixels having a different intensity pattern typical of random static interference. Accurate color segmentation was achieved by initially setting a high color threshold level that included all the foreground pixels and then gradually excluding background pixels from the result image by subsequent iterations of the color segmentation routine at progressively lower tolerance levels.

The color segmentation of autofluorescent estuarine cyanobacteria (Fig. 6c) was the most challenging of the three examples in this first category. The accurate, desired result was achieved by selecting two training pixels (yellow arrows) from the colored regions of foreground objects and then performing automated segmentation iterations at decreasing color tolerance levels starting at 160, followed by 105, 85, and finally 75 to gradually delete background pixels of autofluorescent detritus and smoothen each cell's contour.

The second category of image processing challenge arose when attempting to discriminate populations of microbial cells whose colors were similar or shared significant components, i.e., their foreground pixels occupied overlapping color space within the same image. This category was diagnosed (but not resolved) by splitting the original image into its individual RGB chromatic channels using the "Split to RGB Color Model" function (Fig. 4) and finding (often unexpectedly) that pixels of the same foreground object(s) were present in two or all three images of the displayed color channels.

Three examples illustrate this second color segmentation challenge and its resolution using the improved computing technology. The first occurred when vital staining of a bacterial culture with acridine orange revealed a subpopulation that fluoresced red and another that fluoresced orange. Such was the case for the "AcriOrg-1" test image (Table 1). The algorithm efficiently discriminated these two subpopulations within the same image and produced output images with 99.5% and 98.1% segmentation accuracy of each cells' colored pixels, respectively (Table 2).

The second example for this category arose when using the Molecular Probes Live/Dead® BacLite™ combination of the green fluorescent Syto9 and the red fluorescent propidium iodide stains to examine microbial cell viability based on fluorescent color discrimination as an indicator of membrane integrity. In theory, live cells should fluoresce green because their intact cell membranes only allow passage of Syto9 that ionically bonds to their DNA. In contrast, dead cells should fluorescence red because propidium iodide can permeate their damaged and leaky membranes, and its higher affinity for DNA should displace the Syto9. In practice, however, this classification of cell viability is not always straightforward because some "dead" cells either fluoresce yellow because both stains are intermixed together in the same region within the cell or they have distinctly separated red and green regions of fluorescence within the same cell. The current explanation of this anomaly is that intercalation of propidium iodide between stacked bases in DNA does not always displace the ionic bonding of Syto9 to DNA. Thus, the manufacturer recommends that any presence of red fluorescence should indicate a "dead" cell whose membrane integrity is compromised. Applying the RGB color channel splitting routine to digital live/dead images commonly indicated that the pixels of some predominantly green fluorescent cells actually occupied some red color space (Fig. 7a–d), indicating leaky membranes allowing propidium iodide to enter, and therefore, a visual analysis would erroneously classify them as "live." Non-localized color thresholding applied to the entire images of separated red and green color channels also produced segmented images that yielded erroneous live/dead ratios. Furthermore, since the combinational ratio of the RGB color pixels varied within the individual microbes, selection of a default color range applied to segment the entire image did not accurately fill the color and brightness of each cell for each color stain. CMEIAS image analysis of pixel luminosity per individual cell in the color segmented BacLight-1 image (Table 1) indicated that this problem of intracellular heterogeneity in
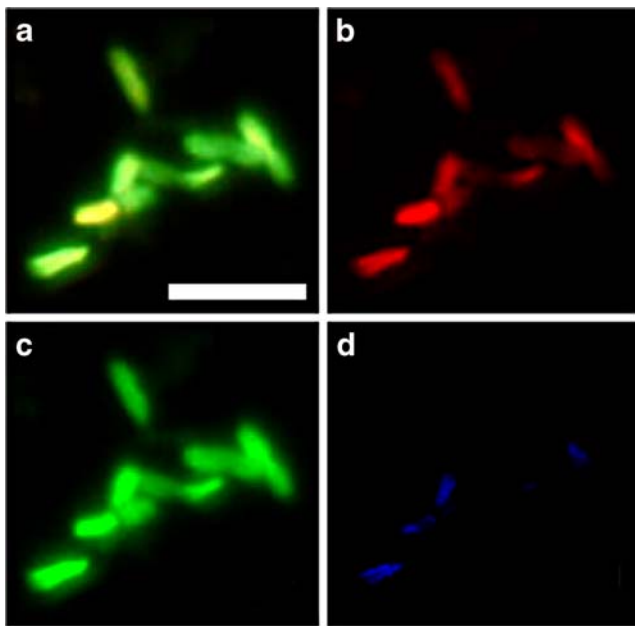
Figure 7 Cells of *Y. pestis* stained with the Live/Dead® BacLite™ reagents to discriminate their viability based on membrane integrity. Cultures were grown to mid-exponential phase at 37°C in brain heart infusion broth, harvested by centrifugation, resuspended in distilled water, stored 7 days at 37°C, stained, and then examined. **a** Original digital image; **b**–**d** the same image split into its red, green, and blue chromatic channels, respectively. *Bar scale*, 2 μm

color intensity was more pronounced with objects of "dead" cells containing some red fluorescent pixels than "live" cells containing only green pixels (Fig. 8).

This color segmentation challenge was resolved by processing the original image into two color-segmented image layers from which the ratio of live/dead cells could be accurately measured. The first segmented image included objects of all "dead" fluorescent cells containing red and yellow pixels as foreground while excluding "live" cells containing only green pixels, and the second segmented image included only objects of green cells as foreground while excluding yellow (and red) cells. The resultant image layers of the foreground pixels in the two color-segmented images were then compared, followed by subtraction of any cells in the green (live) segmented layer that contain overlapping red pixels so no cell was counted twice, i.e., images of live cells only contained green pixels and dead cells contained red/yellow, no overlap. The two resultant segmented images were then flattened and their color-discriminated foreground objects analyzed to measure each group's relative abundance, providing the data to accurately compute the population's live/dead ratio.

To illustrate this application, the relative abundance of live vs. dead cells in a population of *Yersinia pestis* was analyzed to examine their survival following storage in various aqueous environments. The "BacLight-2" image (Table 1) was segmented with high accuracy (Table 2) into

the corresponding pair of color images containing non-overlapping foreground objects and then analyzed by CMEIAS-ImageTool to obtain accurate differential cell counts. The results indicated that membrane integrity of *Y. pestis* cells was preserved in 75.2% of the cells following 7 days of storage in distilled water, yielding a live/dead ratio of 3.03 (*n*=133). Unexpectedly, this level of survival in distilled water surpassed identical treatment of cells stored in the culture medium (47.5% live, live/dead ratio of 0.90, *n*=125) or in 20% glycerol (1.4% live, live/dead ratio of 0.15, *n*=574).

The most complex example illustrating this second category of color segmentation challenge arose when using a combination of multiprobe FISH plus natural autofluorescence to classify multiple microbial phylotypes within the same community image (MRZ-Com), which was a flattened Z-stack of confocal epifluorescence *XY* optisections acquired after applying a multiple-probe FISH protocol to a natural ectomycorrhizosphere community (Table 1 and Fig. 9a). In this case, the same hybridization protocol was applied using several 16S rDNA oligonucleotide probes differing in fluorochrome label and phylogenetic specificity.

This multiprobe FISH image was more complex than most in that it contained red, yellow, and blue cells of interest close to and/or on top of the autofluorescent green fungal hyphae. Mixed colors displayed when multiple fluorescent probes bound to the ribosomal rRNA target in the same cell. The major challenges to accurately segment this image included the diversity of colors representing four different targets of
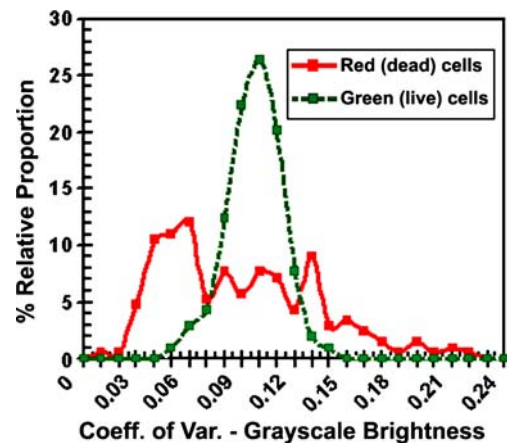

Figure 8 Heterogeneity in intracellular intensity of green and red pixels in images of live and dead cells of a *Micrococcus luteus* and *Bacillus cereus* consortium, respectively. The BacLight-1 image (Table 1) was color-segmented, converted to 8-bit grayscale, and then digitally analyzed to measure the luminosity of all pixels in each individual cell (*n*=418; live/dead ratio of 1:1). Heterogeneity in color intensity is plotted as the percent frequency distribution of cells at constant bin intervals of the coefficient of variation in pixel brightness per cell. The distribution of heterogeneity in luminosity is unimodal in *green* (live cells) and multimodal in *red* (dead cells)

Figure 9 CMEIAS color segmentation of a beech root ectomycorrhizosphere community differentiated by multiprobe FISH and autofluorescence. **a** Whole community epifluorescence micrograph. *Bar scale,* 10 μm. **b**–**e** Color-segmented output images made by the software application showing the in situ spatial distribution of green autofluorescent filaments of the *Fagirhiza pallida* mycorrhizal fungus (**b**); yellow fluorescent *beta-proteobacteria* hybridized with EUB338Mix Cy3 (*red*) and Bet42a Fluos (*green*) probes (**c**); red fluorescent bacteria (gamma-proteobacteria or other non-beta-proteobacteria) hybridized with the Gam42a Cy5 and/or EUB338Mix Cy3 (*red*) probes (**d**); and another unidentified microbial phylotype that exhibits blue autofluorescence but did not hybridize with any of the three fluorescent 16S rRNA-derived oligonucleotide probes (**e**). **a** is reproduced with permission from the American Society for Microbiology Press [7]
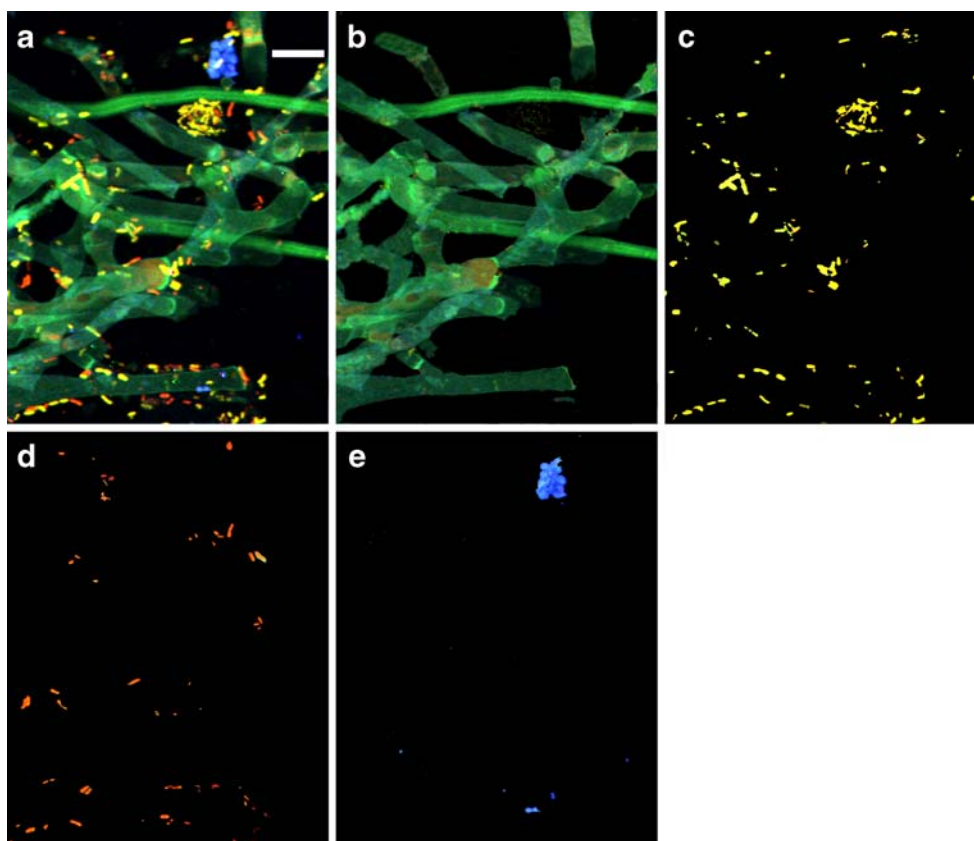
foreground cells, their degree of physical and color overlap, and the broad range of RGB composition for all foreground color pixels. Since most of the object pixels had values in multidimensional color space, simple RGB channel splitting was unable to segment the populations of each phylotype properly. In addition, subtle challenges to accurate color segmentation of the image were the varied luminosity of individual cells, the heterogeneity of colored pixels of the fungal filament structure, and the bleeding of color from bright objects located nearby. These less glaring challenges made selection of a few training pixels insufficient to achieve successful segmentation of the image because the slight irregularity in pixel color and intensity of individual cells caused the segmentation algorithm to include false alarm errors of unwanted pixels in areas of the image that were not close to regions of selected pixels and false dismissal errors of pixels within cells.

This segmentation challenge was solved by careful interactive selection of a more-than-usual number of training pixels from all the regions that contain the same color-discriminated, probe-defined phylotype-specific cells of interest, combined with repetitive 'do' and 'undo' edit testing to optimize the segmentation threshold setting before evoking the color segmentation algorithm. The color segmentations of each population within the community in this complex image are illustrated in Fig. 9b–e.

The user-defined ability to specify the background color of the segmented output image as either pure black or white (Fig. 4) provided an additional tactic to facilitate the segmentation of this complex multiprobe FISH image. When a background pixel was selected in a training sample, the segmentation algorithm forced it and all neighboring pixels to be painted as the background color that extended to the boundary of another region governed by a different selected training pixel. In general, this selection event usually occurred by accident and was easily reversed by the "edit\undo" routine. However, the consequence of intentionally selecting a background pixel was useful in suppressing unwanted pixels from large selected regions in the original image, so long as they did not contain any foreground objects of interest. That criterion was satisfied for this image. When applied, this action successfully excluded noise in large regions of dark background and was particularly useful in removing green pixels of the autofluorescent fungal hyphae from the segmented image of yellow bacteria.

CMEIAS image analysis extracted an abundance of quantitative information on microbial community structure from these multiprobe FISH images after they were accurately color-segmented. Evaluation of the analysis data indicated (1) an overwhelming dominance of fungal biomass (97.86% of total), (2) a ranked abundance of different bacterial populations colonized on the fungal hyphae (percent coverage of the

fungal substratum by the yellow β-proteobacteria, red γ-proteobacteria, and blue autofluorescent bacteria were 6.1%, 2.5%, and 1.3%, respectively), and (3) a higher computed diversity (Simpson's inverse dominance indices of 2.428 vs. 2.205) and evenness (J evenness indices of 0.808 vs. 0.675) of this ectomycorrhizosphere community when the microbial abundance component of the computed index was weighted by the metric of cumulative cellular biovolume rather than just cell counts.

These latter results showed that the increased individual cell size of some prokaryotic phylotypes compensated for their less numerically abundant populations, with the consequence that the computed indices of community diversity and evenness were higher when microbial abundance was weighted by cell biovolume and that CMEIAS-acquired data on both size and number of individual cells worked well together as measures of microbial abundance when computing various indices of microbial community structure. The same trend occurred when CMEIAS allometric scaling was included in a polyphasic analysis of microbial community stability and resilience during ecological succession of methanogenic bioreactors perturbed by a high nutrient loading [10, 16, 19] and during the seasonal dynamics of epilithic biofilm communities in river streambeds [12]. The example reported here shows how the system processed complex images to significantly enhance an in situ analysis of microbial community structure using 16S rRNA-based multiprobe FISH and autofluorescence combined with CMEIAS quantitative image analysis at single-cell resolution.

The third category of challenge in color segmentation arose when the background was of similar color as foreground pixels but present at lower density and with variable luminosity. This type of segmentation problem occurred when processing color images acquired to study the in situ spatial scale of *Pseudomonas putida* cell-to-cell communication mediated by their production and perception of *N*-acylhomoserine lactone (AHL) signal molecules during early biofilm colonization of autofluorescent, plant rhizoplane substrata [14]. That study provided direct in situ evidence indicating that AHL-mediated cell-to-cell communication occurred not only within dense bacterial populations but also in very small groups and over long distances between individual bacteria, and therefore, this cellular activity was more commonplace and effective than previously predicted [14].

In images used for that study, background pixels of the autofluorescent root substratum occupied the same color space as foreground pixels of the red and green fluorescent reporter bacteria but at less density and luminosity, creating a very complex challenge in color segmentation for accurate image analysis that could not be resolved using previously existing software. Here, the system segmented the bacteria in those images with a pixel error rate of 0.28±

0.07% (mean ± SD, $n=3$) in tests to evaluate its performance accuracy (Table 2).

Since the Gfp made by the AHL sensor strain is short-lived in vivo ($t_{1/2}=30–120$ min) due to rapid protease degradation, cell-associated green fluorescence represents a fairly recent reporting of AHL-activated induction of *gfp* [14]. In this case, the intensity of green fluorescence due to intracellular accumulation of Gfp can serve as a quantitative measure of *gfp* gene expression by individual bacteria in situ. Thus, another useful application of this system was to produce images from which the luminosity of each individual cell could be accurately measured in situ. An example is shown in Fig. 10a, b where the AHL-activated green fluorescent cells in the original image were segmented using our new system, then converted to their correspond grayscale objects, thresholded to produce the annotated image with each object numbered, and finally analyzed to compute the mean luminosity value of all pixels in each individual cell in situ. The results (Fig. 11a) indicated that the mean cell luminosity of green fluorescence (≈intensity of AHL-activated *gfp* gene expression) varied considerably among individual AHL sensor cells (ranging between 100 and 218 on a brightness scale of 0–255) and had a left-skewed (skewness=−0.64, $n=71$) distribution containing seven fully resolved plus three partially resolved subpopulations of cells sorted according to their mean luminosity value.

Close inspection of the original color and the segmented, annotated images (Fig. 10a, b, respectively) indicated that this ecophysiological response to the AHL signal molecules was stronger when the sensor cells were located near high
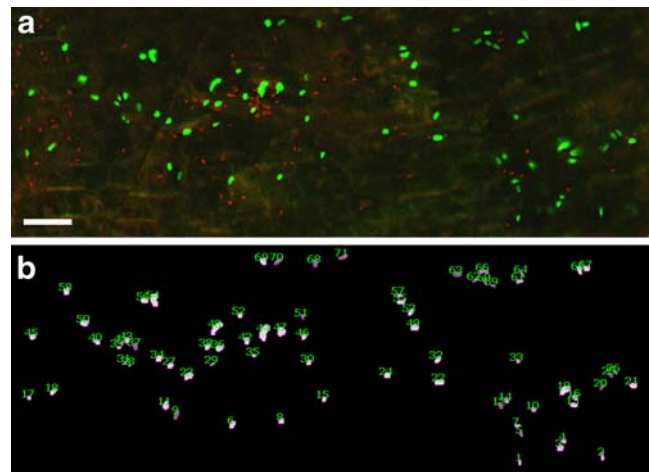

Figure 10 a–b Application of the color segmentation system to produce images for quantitative studies of the in situ spatial scale of gene expression and cellular communication within young biofilms at single-cell resolution. **a** Original image showing cells of the red fluorescent AHL source strain and the green fluorescent AHL sensor strain colonized on a tomato root surface. *Bar scale*, 10 μm. **b** Corresponding annotated grayscale image of the color-segmented AHL sensor bacteria expressing Gfp
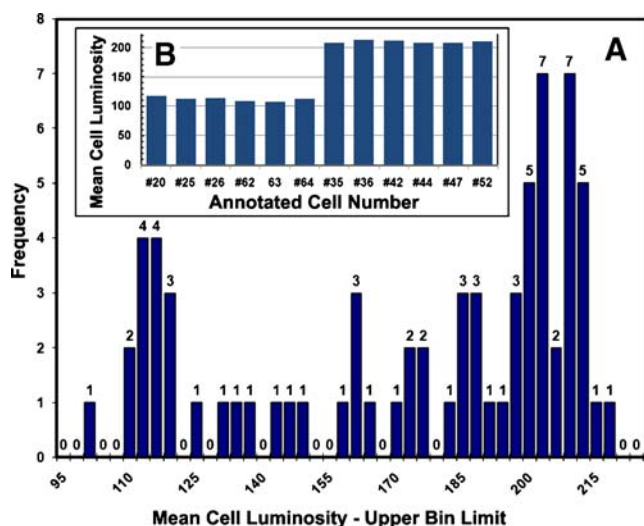
Figure 11 a Frequency histogram of the mean luminosity value extracted from each individual, annotated, green fluorescent AHL sensor cell in Fig. 10b. **b** (*insert*) Bar chart for two groups of cells (identified by their *annotated numbers*) differing in cell luminosity. Brightness values of luminosity reflect the intensity of gene expression of Gfp in individual cells of the green fluorescent sensor strain activated by the uptake of external AHL signal molecules as a measure of bacterial cellular communication

local densities of AHL source cells. For example, green fluorescent AHL sensor cells assigned the annotated numbers of 35, 36, 42, 44, 47, and 52 were located near a high local density of red fluorescent AHL source cells and had higher mean luminosity values than AHL sensor cells assigned annotated numbers of 20, 25, 26, 62–64 that were located in regions of the rhizoplane with lower local densities of AHL source cells (Fig. 11b, insert). These quantitative data provide new further evidence supporting the earlier proposed model predicting that spatial positioning within diffusing AHL gradients was a major factor governing this type of cell-to-cell communication for sessile bacteria [14]. These examples illustrate how this improved computing technology can facilitate in situ microbial ecology studies designed to quantitate the spatial scale and intensity of gene expression and cellular communication within young biofilms, all at individual single-cell resolution.

Related to the above application, our new system should be able to facilitate studies that utilize strains engineered with more stable versions of GFP as "life history reporters" to measure microbial growth rates in situ. This approach is based on quantitative measurements of the reduction in luminosity of GFP per cell (i.e., rate of dilution through cell doubling) after its inducible synthesis is shut down while the population continues to grow [18].

The final category of challenge in color segmentation arose when fluorescence in situ hybridization of 16S rRNA oligonucleotide probes was combined with microautoradiography (FISH-MAR) to detect metabolically active,

microbial populations of specific ribotypes within communities at spatial scales relevant to bacteria, thereby directly linking their phylogenetic identity and activity in complex environments [5, 17, 20]. Microautoradiography relies on the uptake of selected radiolabeled substrates by cells, their assimilation into macromolecules, and their detection as decaying radio isotopic products via exposure of a thin layer of highly sensitive photographic emulsion. Silver grain clusters surrounding bacterial cells indicate active cellular incorporation of the radiolabeled substrates that can be differentiated from neighboring bacteria unable to metabolize the same labeled substrate.

The crucial steps of image processing required for this in situ analysis include those described earlier for color segmentation of probe-defined bacterial ribotypes in FISH images, plus others required to produce the corresponding microautoradiographic images with co-localization of foreground clustered silver grains relative to the density of background silver grains unassociated with the microbial targets. In the typical protocol, microautoradiography of the foreground objects and sample background is addressed by manually inscribing polygons of their cell border on the digital image, followed by counting the silver grains and measurement of the enclosed areas within those polygons. Since commonly performed manually, these crucial steps can be tedious and inconsistent. In contrast, our system accurately produced the output FISH images containing only the foreground object pixels, and then these segmented color images were used to isolate selected regions of the corresponding microautoradiography images containing only the co-localized silver grains of the foreground objects without having to draw the digital areas of interest manually. In this way, the tedious and potentially inconsistent manual steps were eliminated from the protocol, and the segmented output images accurately retained the size and shape of the unaltered foreground objects in a noise-free background, ready for accurate quantitative image analysis.

The pair of FISH-MAR images used to illustrate this application (Fig. 12a, b) were from an elegant study to analyze the in situ utilization of [^{14}C]-labeled pyruvate by two different ribotypes of nitrifying bacteria in a biofilm developing within a wastewater treatment bioreactor [5]. The first step was to convert the dual-probed color FISH image into two color-segmented images: one with the red fluorescent probe specifically hybridized to *Nitrospira* sp. and the other with the green fluorescent probe hybridized to ammonia oxidizers. The corresponding red and green color-to-gray output images with a noise-free background are shown in Fig. 12c, e, respectively. The interesting imaging challenge for this first segmentation step was how to address the yellow-colored pixels in both red and green segmentations while including the foreground object areas that weakly fluoresced with only one color. These weaker signals from
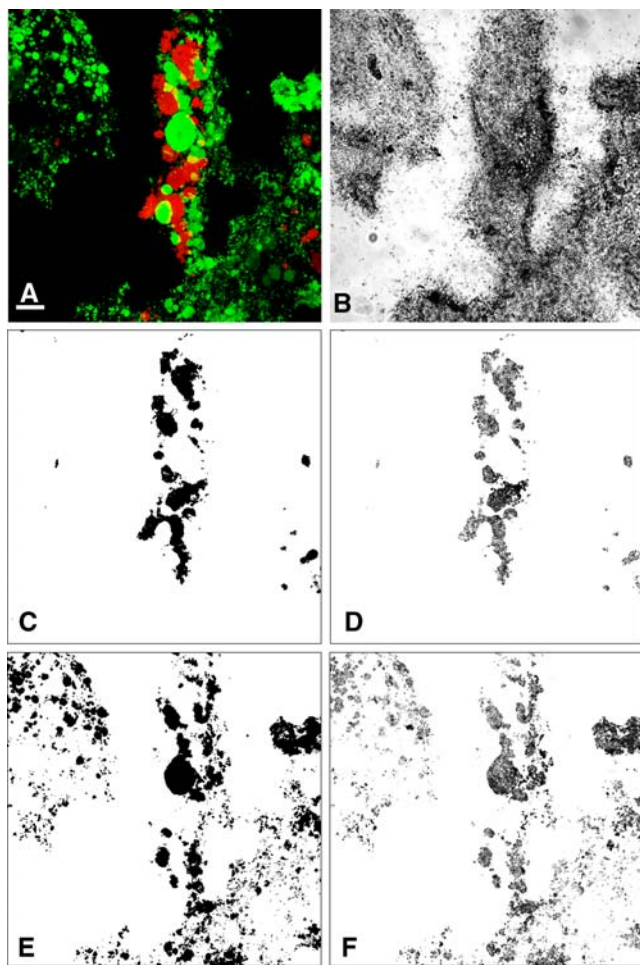
Figure 12 a–f Application of the color segmentation system to process images for in situ FISH-MAR in a flattened stack of confocal images of a nitrifying biofilm in a wastewater treatment bioreactor. **a** Multiprobe FISH image of *Nitrospira* (*red*) and other ammonia oxidizers (*green*). *Bar*, 10 μm. **b** Microautoradiography (*MAR*) image of active utilization of [^{14}C]-pyruvate by the biofilm. **c**, **e** Binary images of the red (**c**) and green (**e**) fluorescent ribotypes isolated by color segmentation of the original FISH image. **d**, **f** Grayscale images of silver grain density corresponding to the two distinct ribotypes isolated from the original MAR image

the foreground objects would have been erroneously eliminated from both output images if segmentation were based on an RGB channel splitting and thresholding procedure, inevitably increasing the error of quantitative

measurements extracted from them. The ability of our new system to perform local-weighted segmentation made it possible to selectively include the faint single-colored areas while simultaneously avoiding the overlapping double-colored areas, thus ensuring that no fluorescent metabolically active biomass was omitted because it did not categorize neatly into either the red or green color channels.

The second step of the improved protocol produced the final segmented, microautoradiographic images. The separate red and green output color-segmented images were transformed into corresponding binary masks where the foreground colored pixels were transparent and all other remaining image pixels were blocked. This "masked" image was the digital equivalent of physically cutting the areas of a selected color out of a printed picture, enabling one to see straight through them. Then, the masked images were layered over copies of the original microautoradiographic image, so the areas containing clusters of silver grains derived only from the colored cells of interest remained in the image while all other silver grains produced by cells stained with the other probe plus all background were accurately and fully excluded. This latter image processing step was performed using the freely available GIMP imaging application to produce the two final radiographs made by the corresponding ribotypes in the community image (Fig. 12d, f).

Typical quantitative measurements extracted from segmented FISH-MAR images are the average diameter and shape of FISH-positive cell aggregates, silver grain intensity of the background for noise subtraction, and the number of silver grains per cell, per constant cell length (for filaments), or per microcolony cluster area [5, 20]. Table 3 lists five additional quantitative biometrics of ecophysiological relevance to a FISH-MAR analysis that were extracted by CMEIAS image analysis of the probe-defined, color-segmented, background-corrected, biofilm images. The cumulative biovolumes of cell clusters (mostly spherical) indicated an approximate 1:2 ratio in biomass of *Nitrospira* sp. vs. other ammonia oxidizers in this image, although *Nitrospira* sp. covered only approximately one fourth of the biofilm area occupied by all ammonia oxidizers on the clay bed substratum in this sample. Correspondingly, the relative amount of pyruvate assimilated by *Nitrospira* sp. (computed from the sum gray metric

Table 3 Ecophysiological characteristics extracted from images acquired using the FISH-MAR technique on nitrifier bacteria assimilating ^{14}C-pyruvate within biofilms and processed using the CMEIAS color segmentation software

Corresponding images are Fig. 12a–f

CMEIAS image analysis Measurement parameter	*Nitrospira* (A)	Other NH$_3$ Oxidizers (B)	Ratio A/B
Cumulative biovolume (μm^3)	1,366	2,929	0.466
% Substratum coverage	4.86	13.93	0.35
Sum gray level	1,490,221	4,193,849	0.355
Microdensitometry index (SumGray*Area)	890,962,900	3,607,133,719	0.247
Grain intensity (SumGray/Area)	2,493	4,876	0.511

applied to an inverted image of the target) was about one fourth that of the other ammonia oxidizers, reflecting a combination of its lower integrative microdensitometry level weighted by its higher silver grain density. These examples illustrate significant new applications of our system for preparing images accurately so that they could be used for quantitative in situ studies of microbial biogeography and metabolic activity at spatial scales relevant to the organisms and their ecological niches.

Concluding Statements

The major challenge of processing color images for quantitative analysis is the difficulty of separating foreground objects along fine delineations of their color and location within the image. This study introduces an improved computing technology that solves—with unprecedented accuracy—many of these complex challenges encountered when using color to discriminate features of significant importance to microbial ecology in digital images. Its various utilities broaden the range of complex color images that can be processed accurately for quantitative analysis of cell size, morphology, abundance, luminosity, and spatial location, thereby adding to the arsenal of tools freely available to microbial ecologists to study their favorite organism or process in situ. The system's ability to vary the color tolerance and uniquely perform localized color segmentation provide the level of increased flexibility required to process the typically complex micrograph images acquired from real-world environmental samples. This flexibility allows the introduced system to succeed in segmenting foreground cells in color images that other existing software, including our earlier prototype of this one, deemed unworkable. All these features reduce the user's time and labor required to accurately perform this tedious yet essential image editing step, hence facilitating the whole process of digital image analysis. As with all applications of quantitative image analysis, accuracy depends foremost on the quality of the acquired primary image and requires that it be high.

This improved color segmentation technology pushes the interface between investigative computing tools and microbial ecology, and its various applications will inevitably lead to new questions as it has already begun to answer old ones [3, 6, 7, 14]. Most importantly, it will assist studies that use color to reveal important quantitative information on the ecology of microorganisms at single-cell resolution, e.g., understanding bacterial individuality to explore the mechanisms through which ecological systems work, how individual cells interact with each other and their environment, and tests of the emerging theory of individual-based modeling and ecology which predict that individual cell

variation is a major driver of population structure and function [8, 15]. The importance of accurately defining microbial processes at the proper spatial scale in which they occur is recognized more and more as ecological theory is deployed to gain a full understanding of microbial ecology [21]. Thus, among the most significant applications of this improved technology will be its use in computer-assisted microscopy to define the spatial scale at which ecologically important events occur among individual, single cells. Finally, the utility of this system applies not only to microbiology but also extends to other disciplines (e.g., eukaryotic cell biology, biomedical imaging, clinical pathology, diagnostic cytology, forensics, remote sensing, geology, astronomy, astrobiology, plant and animal ecology, agronomy, turfgrass science, etc.) where one needs to segment pixel regions of similar but non-identical colors and use color differentiation/classification as a basis for extracting accurate information using digital image analysis.

This improved computing technology is implemented into a software package ready for public release for research, diagnostic, and educational applications. The executable file, user manual, and tutorial images are provided at http://cme.msu.edu/cmeias. The program is a component of the CMEIAS© suite of integrated software whose combined mission is to strengthen microscopy-based approaches for advancing a greater understanding of microbial ecology at single-cell resolution and spatial scales relevant to the organisms themselves.

References

1. Alvarez-Borrego J, Mourino R, Cristobal G, Pech-Pacheco J (2000) Invariant optical color correlation for recognition of *Vibrio cholera*. 01. IEEE Int Conf Pattern Recognition 2847:283–286
2. Chavez de Paz LE (2009) Image analysis software based on color segmentation for characterization of viability and physiological activity of biofilms. Appl Environ Microbiol 75:1734–1739
3. Chi F, Shen SH, Cheng HP, JingYX YYG, Dazzo FB (2005) Ascending migration of endophytic rhizobia from roots to leaves inside rice plants and assessment of their benefits to the growth physiology of rice. Appl Environ Microbiol 71:7271–7278
4. Daims H, Wagner M (2007) Quantification of uncultured microorganisms by fluorescence microscopy and digital image analysis. Appl Microbiol Biotechnol 75:237–248
5. Daims H, Nielsen J, Nielsen P, Schileifer KH, Wagner M (2001) In situ characterization of *Nitrospira*-like nitrite-oxidizing bacteria active in wastewater treatment plants. Appl Environ Microbiol 67:5273–5284

6. Dazzo FB (2004) Applications of quantitative microscopy in studies of plant surface microbiology. In: Varma A, Abbott L, Werner D, Hampp R (eds) Plant surface microbiology. Springer, Germany, pp 503–550

7. Dazzo FB, Schmid M, Hartmann A (2007) Immunofluorescence microscopy and fluorescence in situ hybridization combined with CMEIAS and other image analysis tools for soil- and plant-associated microbial autecology. In: Garland J, Hurst C, Lipson D, Mills A, Stetzenbach L, Crawford R (eds) Manual of environmental microbiology, 3rd edn. American Society for Microbiology Press, Washington, pp 712–733

8. Dethlefsen L, Relman DA (2007) The importance of individuals and scale: moving towards single-cell microbiology. Environ Microbiol 9:8–10

9. Dubuisson MP, Jain AK, Jain MK (1994) Segmentation and classification of bacterial culture images. J Microb Meth 19:279–295

10. Fernandez A, Hashsham S, Dollhopf D, Raskin L, Glagoleva O, Dazzo FB, Hickey R, Criddle C, Tiedje JM (2000) Flexible community structure correlates with stable community function in methanogenic bioreactor communities perturbed by glucose. Appl Environ Microbiol 66:4058–4067

11. Forero MG, Sroubek F, Cristobal G (2004) Identification of tuberculosis bacteria based on shape and color. Real Time Imaging 10:251–262

12. Fukuda M, Matsuyama J, Katano T, Nakano S, Dazzo FB (2006) Assessing primary and bacterial production rates in biofilms on pebbles in Ishite Stream, Japan. Microb Ecol 52:1–7

13. Fuh CS, Cho SW, Essig K (2000) Hierarchical color image region segmentation for content-based image retrieval system. IEEE Trans Image Process 9:156–162

14. Gantner S, Schmid M, Dürr C, Schuhegger R, Steidle A, Hutzler P, Langebartels C, Eberl L, Hartmann A, Dazzo FB (2006) In situ spatial scale of calling distances and population density-independent N-Acylhomoserine lactone mediated communication by rhizobacteria colonized on plant roots. FEMS Microbiol Ecol 56:188–194

15. Grimm V, Railsback SF (2005) Individual-based modelling and ecology. Princeton University Press, Princeton, p 428

16. Hashsham S, Fernandez A, Dollhopf S, Dazzo FB, Hickey R, Tiedje JM et al (2000) Parallel processing of substrate correlates with greater functional stability in methanogenic bioreactor communities perturbed by glucose. Appl Environ Microbiol 66:4050–4057

17. Lee N, Nielsen PH, Andreasen K, Juretschko S, Nielsen J, Schleifer K et al (1999) Combination of fluorescent in situ hybridization and microautoradiography—a new tool for structure–function analyses in microbial ecology. Appl Environ Microbiol 65:1289–1297

18. Leveau JJ, Loper JE, Lindow SE (2007) Reporter gene systems useful in evaluating in situ gene expression by soil- and plant-associated bacteria. In: Garland J, Hurst C, Lipson D, Mills A, Stetzenbach L, Crawford R (eds) Manual of environmental microbiology, 3rd edn. American Society for Microbiology Press, Washington, pp 734–747

19. Liu J, Dazzo FB, Glagoleva O, Yu B, Jain A (2001) CMEIAS: a computer-aided system for the image analysis of bacterial morphotypes in microbial communities. Microb Ecol 41:173–194

20. Nielsen J, Christensen D, Kloppenborg M, Nielsen P (2003) Quantification of cell-specific substrate uptake by probe-defined bacteria under in situ conditions by microautoradiography and fluorescence in situ hybridization. Environ Microbiol 5:202–211

21. Prosser JI, Bohannan BJ, Curtis TP, Ellis RJ, Firestone MK, Freckleton RP, Green JL, Green LE, Killham K, Lennon JJ, Osborn AM, Solan M, van der Gast CJ, Young JP (2007) The role of ecological theory in microbial ecology. Nature Rev Microbiol 5:384–392

22. Reddy CK, Dazzo FB (2004) Computer-assisted segmentation of bacteria in color micrographs. Microscopy Anal 18:5–7

23. Reddy CK, Liu FI, Dazzo FB (2003) Semi-automated segmentation of microbes in color images. In: Eschbach R, Marcu G (eds) Color imaging VIII: processing, hardcopy, and applications. Proc SPIE–International Society for Optical Engineering and The Society for Imaging Science and Technology, vol 5008, Bellingham, Washington, pp 548–559

24. Shopov A, Williams SC, Verity PG (2000) Improvements in image analysis and fluorescence microscopy to discriminate and enumerate bacteria and viruses in aquatic samples. Aquatic Microb Ecol 22:103–110

25. Sieracki ME, Reichenbach SE, Webb KL (1989) Evaluation of automated threshold selection methods for accurately sizing microscopic fluorescent cells by image analysis. Appl Environ Microbiol 55:2762–2772

26. Wilkinson MH, Schut F (1998) Digital image analysis of microbes: imaging, morphometry, fluorometry, and motility techniques and applications. Wiley, UK

27. Witten IH, Frank E (2005) Data mining: practical machine learning tools and techniques, 2nd edn. Morgan Kaufmann, San Francisco, p 525

28. Wyszecki G, Styles WS (1982) Color science: concepts and methods, quantitative data and formulae, 2nd edn. Wiley, NY

29. Zhou J, Fang X, Ghosh BK (1996) Multiresolution filtering with application to image segmentation. Math Comp Modeling 24:177–195

30. Zhou Z, Pons M, Raskin L, Ziles J (2007) Automated image analysis for quantitative fluorescence in situ hybridization with environmental samples. Appl Environ Microbiol 73:2956–2962